Science of the Total Environment 908 (2024) 168450

Contents lists available at ScienceDirect

Science of the Total Environment

journal homepage: www.elsevier.com/locate/scitotenv

Climatic controls on the dynamic lateral expansion of northern peatlands and its potential implication for the 'anomalous' atmospheric CH_4 rise since the mid-Holocene

Haijun Peng [a,b,*], Jelmer J. Nijp [c,d], Joshua L. Ratcliffe [b], Chuxian Li [b], Bing Hong [a,h], William Lidberg [b], Mengxiu Zeng [e], Dmitri Mauquoy [f], Kevin Bishop [g], Mats B. Nilsson [b]

[a] State Key Laboratory of Environmental Geochemistry, Institute of Geochemistry, Chinese Academy of Sciences, 550081 Guiyang, China
[b] Department of Forest Ecology and Management, Swedish University of Agricultural Sciences, 901 83 Umeå, Sweden
[c] KWR Water Research Institute, Ecohydrology Group, Nieuwegein, the Netherlands
[d] Wageningen University, Soil Physics and Land Management Group, Wageningen, the Netherlands
[e] College of Geography and Environmental Sciences, Zhejiang Normal University, 321004 Jinhua, China
[f] School Geosciences, University of Aberdeen, AB24 3UF, Scotland, UK
[g] Department of Aquatic Sciences and Assessment, Swedish University of Agricultural Sciences, 75007 Uppsala 12, Sweden
[h] CAS Center for Excellence in Quaternary Science and Global Change, Xi'an 710061, China

HIGHLIGHTS

- Peatland lateral expansion rate reconstructed from intensive peat depth measurement
- The lateral expansion is non-linear, and the rate has been generally increasing.
- Solar irradiance and ice-rafted debris impact abrupt slow down of lateral expansion.
- Dynamic increment of northern peatland area is likely to dominate CH_4 variations.

GRAPHICAL ABSTRACT

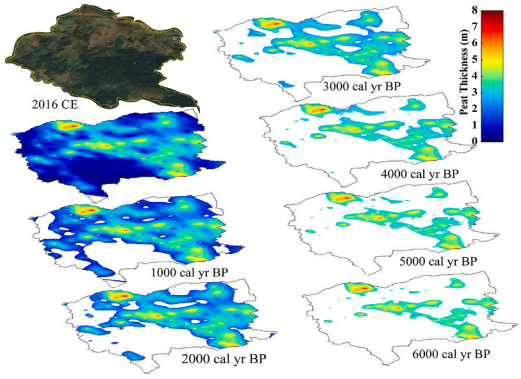

ARTICLE INFO

Editor: Jan Vymazal

Keywords:
Methane
Holocene
Peatland
Lateral expansion
Climate control

ABSTRACT

Understanding the dynamic changes in peatland area during the Holocene is essential for unraveling the connections between northern peatland development and global carbon budgets. However, studies investigating the centennial to millennial-scale process of peatland expansion and its climate and environmental drivers are still limited. In this study, we present a reconstruction of the peatland area and lateral peatland expansion rate of a peatland complex in northern Sweden since the mid-Holocene, based on Ground Penetrating Radar measurements of peat thickness supported by radiocarbon (^{14}C) dates from four peat cores. Based on this analysis, lateral expansion of the peatland followed a northwest-southeast directionality, constrained by the undulating post-

* Corresponding author at: State Key Laboratory of Environmental Geochemistry, Institute of Geochemistry, Chinese Academy of Sciences, 550081 Guiyang, China.
E-mail address: penghaijun@mail.gyig.ac.cn (H. Peng).

https://doi.org/10.1016/j.scitotenv.2023.168450
Received 6 September 2023; Received in revised form 7 November 2023; Accepted 7 November 2023
Available online 13 November 2023

glacial topography. The areal extent of peat has increased non-linearly since the mid-Holocene, and the peatland lateral expansion rate has generally been on the rise, with intensified expansion occurring after around 3500 cal yr BP. Abrupt declines in lateral expansion rates were synchronized with the decreases in total solar irradiance superimposed on the millennial ice-rafted debris events in the northern high latitudes. Supported by the temporal evolution of peatland extent in four other Fennoscandian peatlands, it appears that the northern peatland areal extent during the early to middle Holocene was much smaller compared to previous empirical model reconstructions based on basal age compilations. Interestingly, our reconstruction shows the increments of peat area since the mid-Holocene coincide with the rise in atmospheric CH_4 concentration, and that abrupt variations in atmospheric CH_4 on decadal to centennial timescales could be synchronized with peatland lateral expansion rates. Based on our analysis we put forward the hypothesis that lateral expansion of northern peatlands is a significant driver of dynamics in the late Holocene atmospheric CH_4 budget. We strongly urge for more empirical data to quantify lateral expansion rates and test such hypotheses.

1. Introduction

Methane (CH_4) is a potent greenhouse gas that strongly affects atmospheric chemistry and is responsible for ~20 % of the contemporary total radiative forcing of all the long-lived greenhouse gases (Etminan et al., 2016; Peng et al., 2021b). Atmospheric CH_4 concentration has more than doubled from the pre-industrial level of around 700 ppbv to the present concentration of >1850 ppbv. The causes of this rise are well understood and are largely attributed to increases in anthropogenic emissions such as fossil fuels extraction and transportation, agriculture, and landfills/waste management (Kirschke et al., 2013; Saunois et al., 2020). However, the 'anomalous' increase of atmospheric CH_4 concentration of ~100-ppbv since the mid-Holocene (~5300 cal yr BP), compared to previous interglacial periods, remains intensely debated and poorly constrained (Blunier et al., 1995; Bock et al., 2017; Levine et al., 2011; Ruddiman, 2003; Schmidt et al., 2004). One possible contributor to this anomaly is another disputed issue: the temporal pattern of northern peatlands expansion and the role that northern peatlands have played in the atmospheric CH_4 fluctuations during glacial-interglacial periods and mid-Holocene (Blunier et al., 1995; Nichols and Peteet, 2019; Reyes and Cooke, 2011; Treat et al., 2021). This highlights a fundamental gap in our understanding of the CH_4 cycle and the Earth's climate system.

The currently most accepted hypothesis to explain glacial-interglacial atmospheric CH_4 variations revolves around wetlands, as the dominant natural source of CH_4 (Chappellaz et al., 1993; Frolking and Roulet, 2007; Konijnendijk et al., 2011; Ruddiman et al., 2020). In this hypothesis, the observed interglacial increase in CH_4 is caused by (1) changes in the tropical hydrological cycle and (2) the further development of boreal wetlands after the retreat of continental ice sheets. Together with an intensified CH_4 cycle within terrestrial wetlands in response to higher insolation and temperatures, the development of wetlands would have led to the observed increase in atmospheric CH_4 (Chappellaz et al., 1990; Chappellaz et al., 1997; Schmidt et al., 2004). Although it is generally agreed that wetlands were the dominant natural source of atmospheric methane, the relative contributions of the mid-high northern hemisphere latitudes to the Holocene fluctuations remain an open question (Baumgartner et al., 2012; Sapart et al., 2012; Singarayer et al., 2011).

Northern peatlands represent the largest carbon pool of wetlands in the world and they also release 20–45 Tg CH_4 into the atmosphere annually (Fletcher et al., 2004; Saunois et al., 2020; Zürcher et al., 2013). These emissions strongly affect the content and temporal variations in atmospheric CH_4. Although it is widely acknowledged that northern peatlands were important natural CH_4 sources since the Last Glacial Maximum (LGM; 20,000 years BP), their relative contribution to atmospheric CH_4 dynamics through the Holocene is still the subject of debate (Hopcroft et al., 2017; Nichols and Peteet, 2019; Treat et al., 2019; Zheng et al., 2019). Peatland basal radiocarbon (^{14}C) ages compilation studies have shown that rapid initiation of northern peatlands during the early Holocene coincides with abrupt increases in atmospheric CH_4 concentrations, which implies that the rapid initiation contributed to the sustained peak in CH_4 at this time (MacDonald et al., 2006; Smith et al., 2004; Yu et al., 2010; Yu et al., 2013). However, it is recognized that the temporal structure of peatland initiation is sensitive to sampling biases and treatment of basal peat ^{14}C dates. As a result, peat area estimations based on the compilations might be problematic due to poor quality control on the basal ^{14}C date dataset (Ratcliffe et al., 2021; Korhola et al., 2010; Loisel et al., 2017; Payne et al., 2016; Piilo et al., 2020; Reyes and Cooke, 2011).

Recent findings (Korhola et al., 2010; Treat et al., 2021; Morris et al., 2018; Ehnvall et al., 2023) suggest that the role northern peatlands played in the global CH_4 cycle is substantially different from former assumptions, e.g., MacDonald et al. (2006), Yu et al. (2010), and Smith et al. (2004). Using revised chronologies of peatland initiation for Alaska and the circumpolar Arctic, Reyers and Cooke (2011) revealed that peatland initiation lagged the abrupt increase in atmospheric CH_4 during the early Holocene and thus could, instead, be responsible for the aforementioned later rise in CH_4 in the mid Holocene. Besides, it is suggested that the widespread establishment of peatlands was driven by regionally asynchronous growing season warming (Morris et al., 2018). A recent basal age compilation study even found that the development of northern peatland is nearly completely decoupled from trends in atmospheric CH_4 concentrations during the Holocene (Treat et al., 2021), calling into question the assumptions built into the basal age compilation studies (Loisel et al., 2017; MacDonald et al., 2006; Ratcliffe et al., 2021; Yu et al., 2010), along with the idea that the area of northern peatlands had reached >80 % of the present area extent before the mid-Holocene and the rapid increment of peat area occurred primarily in the early Holocene (e.g. Nichols and Peteet, 2019). On the contrary, when a multi-basal-ages quality control was used in an attempt to eliminate sampling biases, rapid peatland expansion was found to occur only after the mid-Holocene (Korhola et al., 2010).

The basal age compilation method to estimate peatland areal extent was underpinned by the assumption that peatlands expand linearly in time after initiation. However, there is little empirical evidence to support this assumption, which has been called into question (Ehnvall et al., 2023; Loisel et al., 2017; Morris et al., 2018; Ratcliffe et al., 2021). First, the assumption that peatlands expanded linearly through time is dubious because terrestrialization and paludification of peatlands is influenced by a range of biotic and abiotic factors such as regional growing season climate (Morris et al., 2018; Ruppel et al., 2013; Weckström et al., 2010), vegetation succession (Holmquist and MacDonald, 2014; Yu et al., 2013), and especially heterogeneity in landscape morphology (Loisel et al., 2013; van Bellen et al., 2011). Secondly, reconstructions based on frequency histograms of binned calibrated age ranges cannot be downscaled to regional or local scales, which makes it difficult to test the connections between peatland development dynamics and abrupt climate or environmental changes. For instance, the expansion of peatlands on the northern Sweden coastline area on a landscape scale was non-linear and influenced by the wetness of the terrain, in turn determined by the hydro-edaphic properties, for example, topographic roughness and sediment porosity (Ehnvall et al., 2023).

Previous studies based on basal age isochrones have shown that the lateral expansion of single peatlands was not linear on millennial timescales (Korhola, 1994; Mathijssen et al., 2014; Mathijssen et al., 2017; Mathijssen et al., 2016) and indeed the modern-day expansion rate as recently reported is not linear or consistent with earlier rates in the Holocene (Juselius-Rajamäki et al., 2023). However, the links between the dynamics of peatland lateral expansion on centennial-millennial and decadal-centennial timescales, abrupt global climate changes, and topographic features remain understudied. Here, we reconstruct the lateral expansion history of Degerö Stormyr, a boreal oligotrophic mixed mire complex located in northern Sweden (Nilsson et al., 2008), using extensive high-resolution Ground Penetrating Radar (GPR) peat thickness measurements in combination with 89 ^{14}C dates from four peat cores. The specific aims of this study are to (1) reconstruct lateral peatland expansion dynamic at decadal-centennial timescales using fine-resolution GPR measurements of peat thickness, (2) test the assumption of linear lateral expansion of the peatland after establishment, and (3) discuss the implications of centennial timescale abrupt climate changes on the lateral expansion of peatlands and atmospheric CH_4 concentrations.

2. Materials and methods

2.1. Study site

The Degerö Stormyr mire complex (64°11′N, 19°33′E; ~270 m.a.s.l.) is an oligotrophic minerogenic mire covering 6.5 km^2, located approximately 70 km from the Gulf of Bothnia and 60 km north-west of Umeå, capital city of Västerbotten, northern Sweden (Fig. 1A). It is one of the national research infrastructures ICOS (Integrated Carbon Observation System) in Sweden. The peatland consists of a mosaic of interconnected mires which are underlain by glacial islets and ridges (Fig. 1B). The bedrock in the area is gneiss and the climate at the site is defined as cold temperate humid. The landscape of the catchment consists of 70 % mire and 30 % coniferous forest. The mean annual precipitation and air temperature from 1961 to 1990 are 523 mm and 1.2 °C, respectively (Peichl et al., 2014). The hottest and coldest month are July and January, with mean monthly temperatures being 14.7 and −9.5 °C, respectively. The growing season normally covers early May to late October, with the remaining months the site being covered by snow. The microtopography within the Degerö Stormyr catchment is dominated by moss carpets and lawns, with hummocks occurring sparsely. Carpets and lawns are characterized by the dominance of *Sphagnum majus* Russ. C. Jens, and *Sphagnum balticum* Russ. C. Jens, while hummocks are dominated by *Sphagnum fuscum* Schimp. Klinggr. and *Sphagnum rubellum* Wils. The vascular plant community mainly consists of *Vaccinium oxycoccos* L., *Eriophorum vaginatum* L., *Rubus chamaemorus* L. Hartm., *Andromeda polifolia* L., and *Trichophorum cespitosum* L. (Nilsson et al., 2008). Based on Eddy Covariance (EC) measurements, the estimated total CH_4 emission was 9 ± 1.8 g CH_4-C m^{-2} during 2004 and 14 ± 2.5 g CH_4-C m^{-2} during 2005 (Nilsson et al., 2008).

2.2. Peat thickness measurements

Peat thickness was measured by a MALÅ Ground-penetrating Radar (GPR) with a 100 MHz shielded antenna (MALÅ Geosciences, Sweden) in the winter of 2016. The antenna was towed using a snowmobile to move forward for the transect profiling. The spacing between traces was 0.1 m and 16 stacks were used for each trace. The sampling time window was 790 ns, providing a maximum detection depth of 13 m with a vertical resolution of approximately 25-cm. Twenty parallel transects (Fig. 1B) ranging from 500 to 2500 m long were surveyed. The interval of the GPR transects is 100 m and the total length of the transects is around 25 km. The locations and altitudes of the transects were obtained by SWEREF 99, the national geodetic reference systems of Sweden. Major sediment interfaces can cause strong GPR reflections owing mostly to changes in water content which are determined by porosity and organic matter content (Comas et al., 2005; Warner et al., 1990). To verify the accuracy of GPR peat thickness measurements, 85 sites along the 20 transects were manually probed using an iron rod (Nijp et al., 2019) (Fig. 1B).

Time delay between electromagnetic wave transmitting and reception was converted to peat thickness using an average peat velocity of 0.038 m ns^{-1}. To identify the interface between peat and mineral soil,

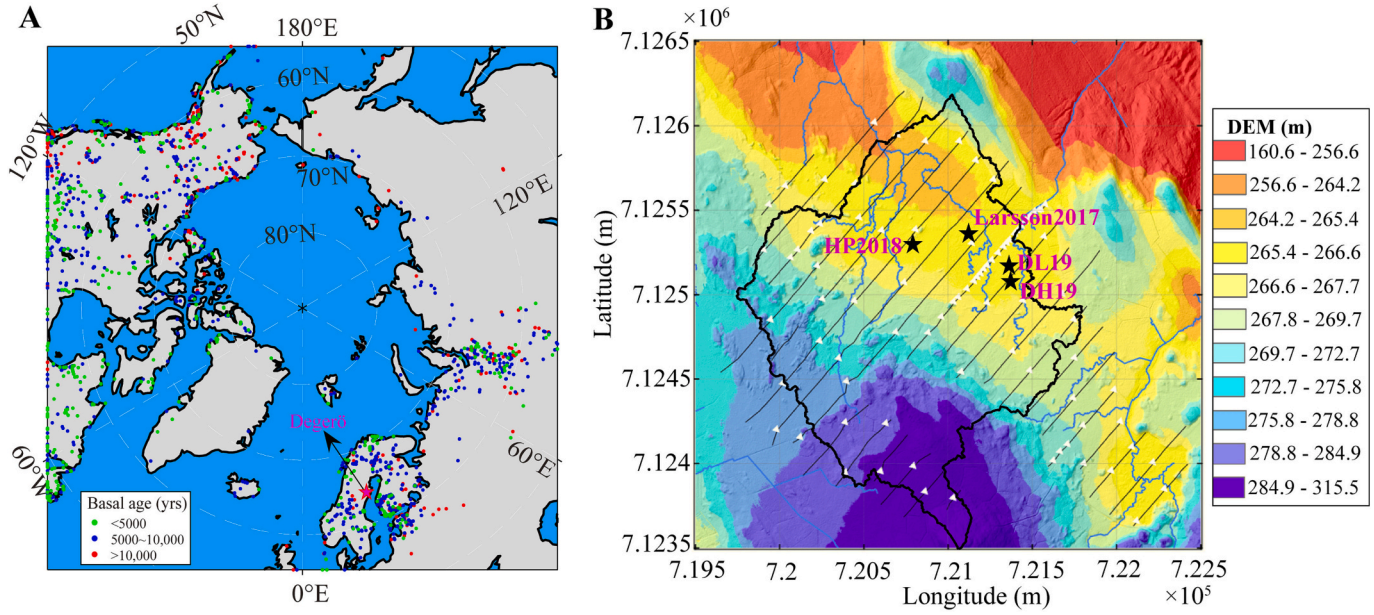

Fig. 1. (A) Locations of Degerö Stormyr mire complex (solid black pentagram) and other northern peatlands with basal ages, peat basal age dates compiled in (Loisel et al., 2017) (red points, blue points, and green points represent sites that are older than 10,000 years, between 5000 and 10,000 years, and younger than 5000 years, respectively); (B) Spatial distribution of the GPR transects (parallel black lines) and locations of the manual probing sites (white solid triangles) using the iron-rod probing method. The four black solid pentagrams show the locations of the peat cores used in this study. The bold black line represents the catchment of Degerö based upon the LiDAR-derived 2-m resolution DEM (Leach et al., 2016).

the raw GPR data were processed in the Reflexw software (Sandmeier Geophysical Research, Germany). Processing steps include: (1) applying time-varying gain to each trace to create equally distributed amplitudes in time axis, (2) using a "De-wow" filter to eliminate low frequencies, (3) using a band-pass filter to eliminate high- and low-frequency noise, (4) applying a static correction to eliminate the time delay between trigger and recording, and (5) applying a static correction to account for peatland topography (Adrian, 2004; Comas et al., 2005). The peat-mineral soil interface was manually interpreted in the Reflexw software based on the strong GPR reflections and exported to peat thickness along the transects at 1 m resolution.

2.3. Peat area extraction

The resolution of the GPR measurements along and between the transects is 1 m and 100 m, respectively. To create an evenly spaced peat thickness grid dataset, the GPR measurements were interpolated into a grid of 1 m resolution using the natural neighbor interpolation, which is based on Voronoi tessellation (Tanemura et al., 1983). An evenly spaced 3000 × 3000 matrix of peat thickness interpolation data was thus computed for further peat thickness distribution mapping and peat area extent extraction. After the interpolation, the peat thicknesses were projected to the 3000 × 3000-m space for peat thickness distribution mapping and peat area extent extraction. The 9 million peat thicknesses, where each thickness measurement represents a 1 m^2 area, were then separated into 800 groups ranging from 1 cm to 800 cm. The calculated number of each peat thickness is the peat area of that thickness, and the area unit is m^2. The cumulative area from 800 cm to 1 cm represents the peatland area evolution dynamics.

2.4. Peat core sampling and peatland lateral expansion rate reconstruction

Four peat cores (Larsson2017, sampled in 2009; HP2018, sampled in 2018; DH19 and DL19, both sampled in 2019) were collected using a Russian peat corer (Fig. 1B). Eighty-nine plant residual samples from the four cores were selected for AMS^{14}C dating and the results are presented in Table S1. The AMS^{14}C data from Core Larsson2017 was reported in Larsson et al. (2017). The AMS^{14}C data from the top one meter of cores DH19 and DL19 were reported in Li et al. (2023). The BACON 2.2 R package (Blaauw and Christen, 2011) was used to simulate the age-depth model. The 89 AMS^{14}C dates with their sampling depths were integrated into one age-depth model representing the Degerö Stormyr peatland complex as these dates are from different locations of the mire and the model has been iterated 1 million times in the BACON method (Blaauw and Christen, 2011). Since the recent peat growth rate is estimated to be around 0.9 cm per year based on both ^{210}Pb dating and a reference cable buried in 1994 (Olid et al., 2014), an extra depth of 9 cm was compensated to the Larsson2018 core to make all the cores have the same starting point. The age-depth model "ALL" (Fig. S1), representing the Degerö Stormyr peatland complex, yields a 56 % coverage of the 89 dates. The accumulation rates (Fig. S2) for the 4 cores as well as the Degerö Stormyr peatland complex (ALL) were calculated based on the age-depth models.

To reconstruct the temporal changes in peat area, we assume that the age-depth model of "ALL" and its uncertainties can generally represent the Degerö Stormyr peatland complex, as it is the middle one among the four age-depth models (Fig. S1). The extracted peat area at each peat depth was converted to the peat area at a certain time based on the age-depth model of "ALL". In the meantime, the spatial distribution of peat thickness at a certain time was also determined based on the relation between peat thickness and the age-depth model. The lateral expansion rate (m^2 yr^{-1}) was calculated using the area difference at two peat thicknesses to divide the age difference at the two thicknesses, which derived from the age-depth model. The uncertainties of the "ALL" age-depth model were treated as the uncertainties of the reconstructions of peat area and lateral expansion rate. To avoid overinterpretation, peat deposits thinner than 40 cm were not analyzed in this reconstruction. Besides, we also compiled peatland expansion reconstructions from published data of three other Fennoscandian peatlands, i.e., Kalevansuo (60°38′49″N, 24°21′23″E, 123 m.a.s.l.) (Mathijssen et al., 2017), Siikaneva (61°50′N, 24°12′E, 160 m.a.s.l.) (Mathijssen et al., 2016), and Lompolojänkkä (68.0°N, 24.2°E, 269 m.a.s.l.) (Mathijssen et al., 2014). Raw data from these 3 studies were also provided in the recent study (Mathijssen et al., 2022). For further comparison, the reconstructed peatland area in this study and the compiled data were normalized against their current peatland area (4.85, 0.14, 12, and 0.9 km^2 for Degerö Stormyr, Lompolojänkkä, Siikaneva, and Kalevansuo, respectively).

2.5. Wavelet correlation analysis

To evaluate the correlation at specific timescales and times, we examined the wavelet-coherence between atmospheric CH_4 concentration and peatland lateral expansion rate based on wavelet analyses (Torrence and Compo, 1998). The time series of both the peatland lateral expansion rate and atmospheric CH_4 concentration was resampled into a one-year resolution using the spline function in MATLAB. The interpolation and wavelet-coherence analysis were conducted in MATLAB 2020b (The MathWorks, Inc., USA).

3. Results

3.1. Peat thickness distribution

The interface between mineral soil and peat was generally sharp and showed high spatial heterogeneity, both when identified through GPR interpretation and manual probing (e.g., L10) (Fig. 2). The root-mean-square error (RMSE) between manual and GPR measurements was 0.58 m. This consistency of high agreement between the two methods becomes clear along transect L10 which has denser manual probing measurements. Generally, the peat thickness is highly variable and undulating throughout the whole studied area (Fig. 2). Taking the extreme example of transect L2, peat thickness varied from <30 cm to over 7 m within a 100-m distance. The surface topography shows high variability, with transects from L10 to L15 were divided into two parts by the forest hill situated in the southwest part of the catchment. Besides, some small hills or ridges are apparent in transects L5, L6, L7, L9, and L10 as well.

Manual probing peat thickness ranged from 0.1 m to 6.53 m, with the median peat thickness being 1.84 m (n = 85). Peat thickness values from manual probing and GPR measurements at locations nearby were highly correlated (r^2 = 0.86; n = 85; RMSE = 0.58 m) (Fig. 3A). Most of the manual and GPR measurements fell near the 1:1 line, showing the accuracy of both methods. It is also clearly shown that hand measurements lead to an underestimation of peat thickness of, on average 0.09 m (Fig. 3A). For some locations the peat thickness estimate by manual probing is considerably smaller than the GPR estimate (e.g., L17; Fig. 2). This difference may be caused by small pieces of wood or root residues blocking the iron rod for further penetration, resulting in an underestimation of peat thickness by hand measurements.

3.2. Spatial distribution of peat thickness

The GPR measured peat thickness ranged from 0 m to 8 m, with the median value being 1.91 m along the transects (n = 24,532). While the median peat thickness at identical locations after the natural neighbor interpolation was 1.92 m (n = 24,532), with the maximum and minimum values being 7.2 and 0.01 m, respectively. This shows that the natural neighbor interpolation peat thicknesses are consistent with the GPR measurements in general. Further linear regression analysis reveals that the GPR measured and interpolated peat thicknesses are highly correlated (r^2 = 0.96; n = 24,532; RMSE = 0.26 m).

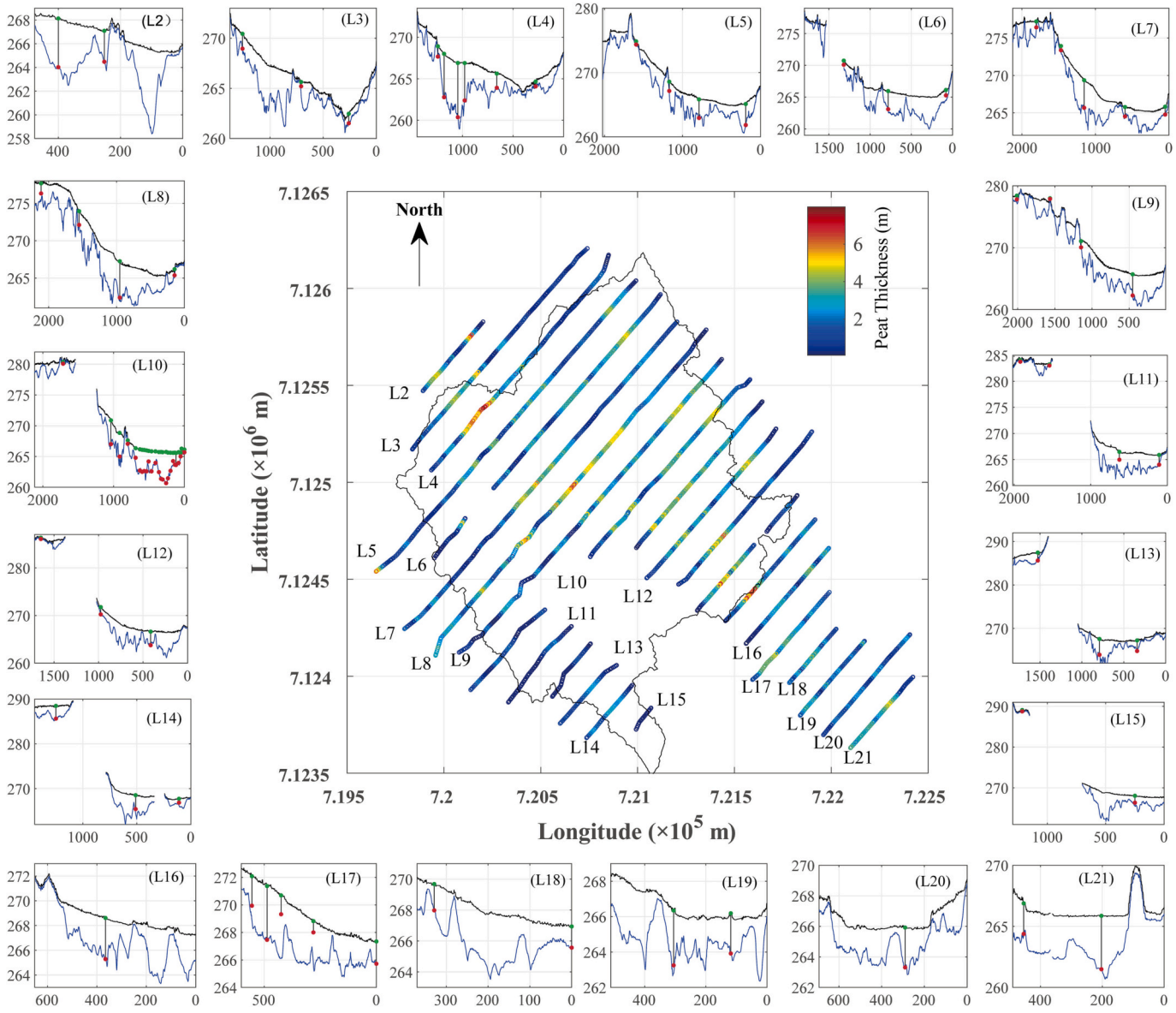

Fig. 2. Peat basin morphology along the 20 GPR transects (surrounding 20 subfigures), and the peat thickness profiles (central figure, the latitude and longitude numbers represent SWEREF99 TM coordinates). From L2 to L21, the X-axis and Y-axis are elevations (m) and distances (m), respectively. The black lines and blue lines in the surrounding subfigures are the surface and bottom of the peat deposit; the green and red dots show the location of the iron rod measurements and the bottom they touched. Notice that the elevation in these sub-figures is not all the same and distance 0 is the location of the most Northwest of the transects.

The spatial distribution of peat thickness is highly heterogeneous, with several centers situated sparsely across the mire. Peat thicker than about 2 m has an overall northwest-southeast directionality (Fig. 4). This directionality is in line with the surface topography of mineral soils surrounding the mire. Locations with thinner peat are often distributed with hills and ridges that can be identified from the topography too (Fig. 1B). The total interpolated area (areas with peat thickness data in Fig. 4) is 4.85 km^2 and the total peat volume is estimated at 8,545,908 m^3. The area-averaged, GPR-measured, and manually measured peat thickness is 1.76 m, 2.05 ± 0.009 m (mean ± standard error), and 2.17 ± 0.156 m (mean ± standard error), respectively. These differences can be explained by differences in sampling strategy (areal coverage and number of measurements). Though peat thickness is up to around 8 m, most of the peat deposits are <2 m thick (Fig. 5A). The cumulative area increases with peat thickness nearly exponentially (Fig. 5B). The area with peat thickness lower than 0.3 m, 1 m, and 1.76 m is 170,292 m^2, 1,519,800 m^2, and 2,689,421 m^2, which account for 4 %, 31 %, and 55 % of the total interpolated area, respectively (Fig. 5A and B).

4. Discussion

4.1. Climatic control on peatland lateral expansion

The climate of the northern high latitudes during the Holocene was characterized by abrupt millennial timescale ice-rafted debris events, known as the Bond Events and the Little Ice Age (LIA) (Bond et al., 1997). The establishment and development of peatlands are largely influenced by abrupt changes in climate (Charman et al., 2013; Yu et al., 2010). A previous study has suggested that the ~1450-yr climate periodicity has been regulating the peatland initiation in western Canada during the Holocene (Campbell et al., 2000). However, the relation between centennial-millennial abrupt climate change and peatland lateral expansion in this region has barely been investigated. Based on our reconstruction, the peatland area of Degerö Stormyr increased over 6 times since the mid-Holocene, with an accelerated increase in both peat area and peat accumulation rate happening during the last 3000 years (Fig. 6A and B). This is consistent with the complex underlying

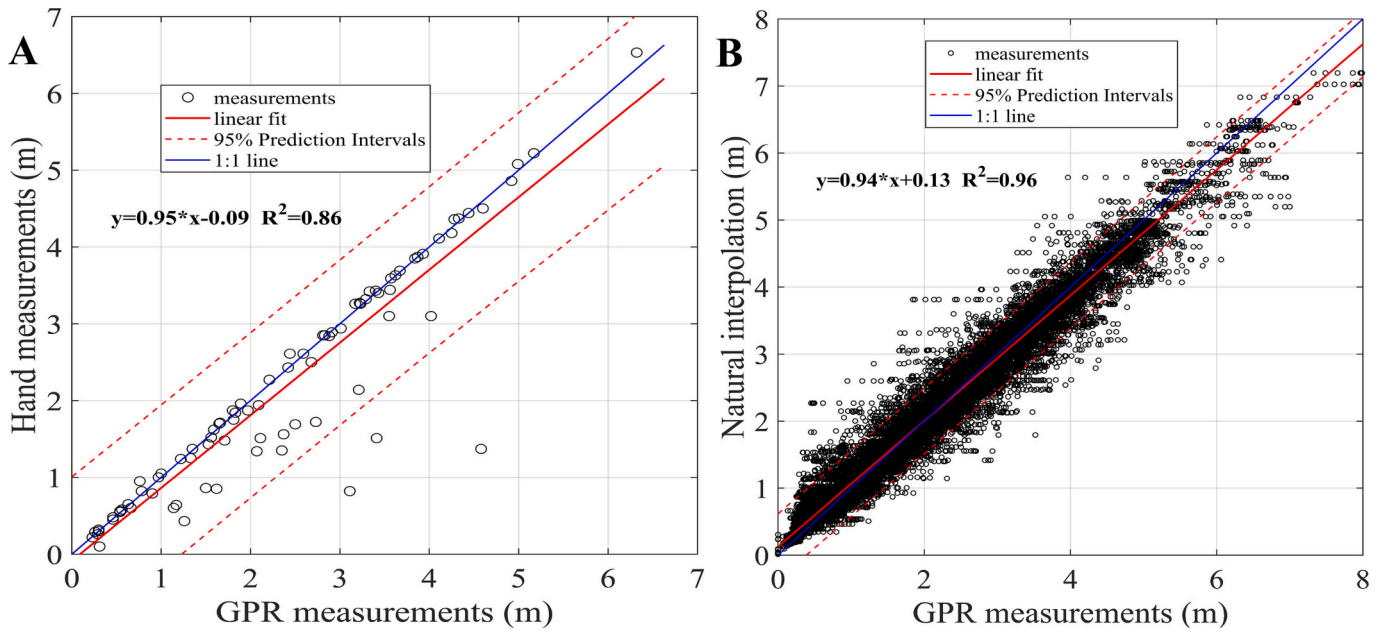

Fig. 3. Correlation between (A) manual iron rod probed and GPR measured peat thickness, (B) natural neighbor interpolated and GPR measured peat thickness.

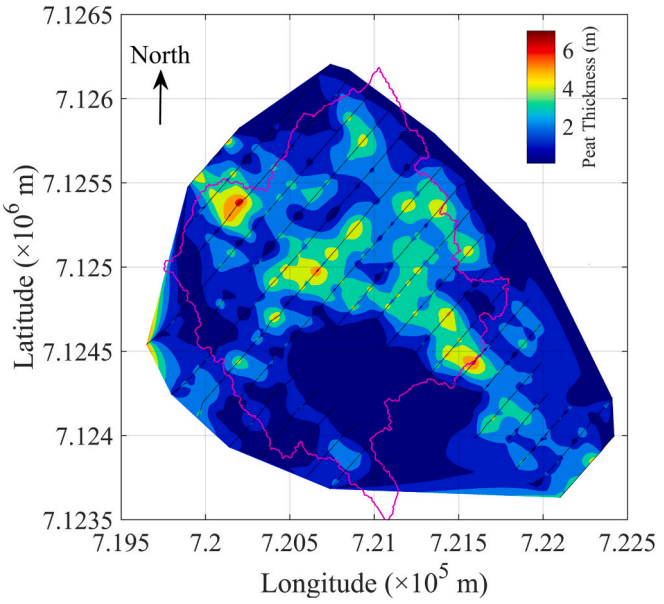

Fig. 4. Three-dimensional interpolated peat thickness model based on the GPR measurements, with black parallel lines showing the location of GPR transects. The magenta line represents the Degerö Stormyr catchment delineated in the previous study (Leach et al., 2016).

topography below the peat surface reported here and in earlier work (Malmström, 1923; Kulczyński, 1949) which would be expected to result in a relatively slow and episodic expansion (Ehnvall et al., 2023; Loisel et al., 2013). We find the lateral expansion rate of Degerö Stormyr has been increasing quadratically in general, with the fastest rates in the mid and late Holocene and with 5 abrupt changes (Fig. 6). These abrupt changes were synchronized with the declines in total solar irradiance (TSI) during the 4 Bond Events and the LIA (Fig. 6B, C, and D). Rapid increases in lateral expansion rates were generally observed during intervals after the cooling events, with accelerated lateral expansion during the Medieval Warm Period (MWP) (700–1000 cal yr BP) and the period after the LIA. The abrupt changes in lateral expansion rate are well synchronized with the decreases in TSI (Fig. 6C and D). Especially, the highest lateral expansion and peat accumulation rates occurred after the end of the LIA and lasted for about 100 years and the abrupt decreases in both parameters that proceeded this time coincided with the Maunder Minimum. This synchrony of events suggests that the lateral expansion of peatland could be linked to both solar activities and millennial northern high latitudes climate fluctuations (see Section 4.4 for summary of uncertainties on these aspects).

The millennial timescale rapid increases in peatland lateral expansion rate could be attributed to the positive impact of warm and wet climate on peatland productivity in the prevalent climatological conditions, thus causing rapid peat development both vertically and horizontally (Charman et al., 2013), with the two processes being somewhat linked in peatlands with complex underlying topography (e.g. Juselius-Rajamäki et al., 2023). Additional pulses of higher peat expansion rates are also associated with the recovery of solar irradiance after a period of depressed activity. This is highly consistent with what we know about peatland lateral expansion processes (Rydin et al., 2013). Peatland expansion or paludification of mineral soil requires the soil to be saturated near-continuously for a period of years to decades (Ivanov, 1981; Ehnvall et al., 2023), this is consistent with increases in growing season soil wetness that would be expected with the lower evapotranspiration and shorter growing season that would accompany reductions in solar irradiance, this is supported by a reconstruction of nearby (<5 km) mire surface wetness that shows the wettest conditions during the maunder minimum (van der Linden et al., 2008). Conversely, once established, warmer conditions and, possibly reductions in catchment water inputs (Sallinen et al., 2023; Ehnvall et al., 2023), may favor peat vertical growth and the persistence of peat on mineral soil, for which the pores have become clogged by organic matter, so called 'proto-peat', during the preceding colder or wetter period (Rydin et al., 2013).

These climate and solar irradiance dynamics also become apparent in the reconstructed peatland lateral expansion rates and peat accumulation rate in our study. Lateral expansion seems to intensify in a warmer climate at around 4800 cal yr BP, which agrees well with literature reporting widespread increased peatland initiation in North America (Gorham et al., 2012; Packalen et al., 2014) and Europe (Edvardsson et al., 2014; Ruppel et al., 2013). In addition, recent studies showed that peatlands in high-latitude northeast China (Xing et al., 2016; Zhang et al., 2022; Zhang et al., 2018; Zhao et al., 2014) and Indonesia (Dommain et al., 2014) have experienced rapid initiation

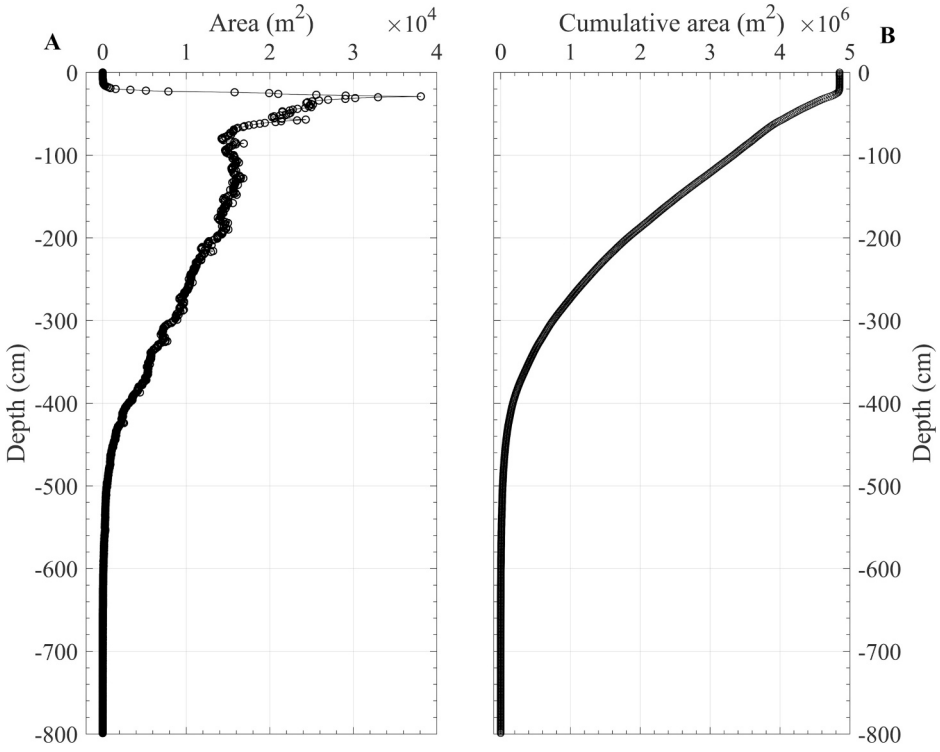

Fig. 5. Peat cover area of Degerö at different peat depths: (A) the expanded peat area, and (B) the cumulative total peat area.

since the mid-Holocene. The hydroclimate that caused these rapid initiations could also have promoted the lateral expansion of established peatlands since then.

The accelerated lateral expansion rate, occurring during the last 2500 years, is consistent with the initiation of numerous shallow peatlands around the northern hemisphere. Previous investigation has shown that most of these peatlands were <2 m deep (Gorham, 1991; Gorham et al., 2012; Hugelius et al., 2020). In our case, >60 % of the Degerö Stormyr peatland is covered by peat that is <2 m thick (Fig. 5). With a late Holocene northern peatland accumulation rate of around 0.07 cm per year (Larsson et al., 2017; Loisel et al., 2014), these peatlands are expected to be initiated during the last three millennia. It has been pointed out that late Holocene shallow peatlands are typically understudied due to a clear bias towards deeper sites in the palaeoecological literature from which most basal ages are derived (Ratcliffe and Payne, 2016). The lack of representation of basal ages from shallow and young peats makes estimations of recent peatland dynamics particularly questionable in previous basal age compilation studies (Korhola et al., 2010; MacDonald et al., 2006; Yu et al., 2010). While acknowledging the uncertainties (see Section 4.4), the estimated increases in lateral expansion rate since the mid-Holocene at Degerö Stormyr seem to be in line with the accelerated peatland initiation and lateral expansion across the northern hemisphere. This suggests that the lateral expansion process may be a major driver of peat areal extent increases since the mid-Holocene.

4.2. Links between dynamics of peatland lateral expansion and atmospheric CH_4

The atmospheric CH_4 concentration in the northern hemisphere showed strong fluctuations throughout the Holocene (Fig. 6F). It reached a minimum at the mid-Holocene (around 5300 cal yr BP) and since then has been generally increasing, with the most rapid increases occurring after around 2500 cal yr BP (Blunier et al., 1995). This general increasing trend in atmospheric CH_4 concentrations agrees well with the areal expansion of the four peatlands compiled in this study, with most of the increase happening during the late Holocene (Fig. 6F and G). In addition, the centennial-millennial timescale changes in atmospheric CH_4 concentration are synchronized with most of the abrupt variations in peatland lateral expansion rate superimposed on the changes of TSI and IRD. For example, both lateral expansion rate and CH_4 concentration experienced a sudden increase and decrease at the beginning and end of Bond event 1, respectively. Abrupt declines in both the estimated lateral expansion rate and CH_4 concentration were presented at the end of MWP and LIA. These abrupt changes could be attributed to either declines in TSI or intensifications in IRD, suggesting global climatic changes or northern high latitudes sea-atmosphere circulations may have played important roles in the process of peatland lateral expansion and hence the variations in atmospheric CH_4 concentrations (Blunier et al., 1995; Hopcroft et al., 2017; Morris et al., 2018). Wavelet coherence analysis shows that the peatland lateral expansion rate of Degerö is significantly correlated to atmospheric CH_4 concentration on a ~20-yr timescale throughout the mid-Holocene, while the correlations were also significant at around 2500 and 500 cal yr BP on a ~100-yr timescale (Fig. 6H). These periodicities and their wavelet coherences in the time domain indicate the decadal-centennial changes in atmospheric CH_4 concentrations might be contingent on the lateral expansion dynamics of northern peatlands, which are subjected to solar activities and hydroclimate changes in the northern high latitudes.

It is worth noting that differences exist between the single peatland historical areal extent reconstructions. Degerö Stormyr and Lompolojänkkä show similar expansion trends but differ from Kalevansuo and Siikaneva (Fig. 6G). Despite the different morphological settings that are expected to control lateral expansion, the development of at least Lompolojänkää is remarkably similar to Degerö. Interestingly, despite the differences across the four sites, all single-peatland-based reconstructions show far smaller peat areal extent at the mid-Holocene than the previous global and regional estimates based on compiled basal peat ^{14}C dates (MacDonald et al., 2006; Spahni et al., 2013). Since basal age compilation studies were largely uncertain due to data availability and mismatched representative peatland in areas such as northern Europe and the Western Siberian Lowlands (Loisel et al., 2017;

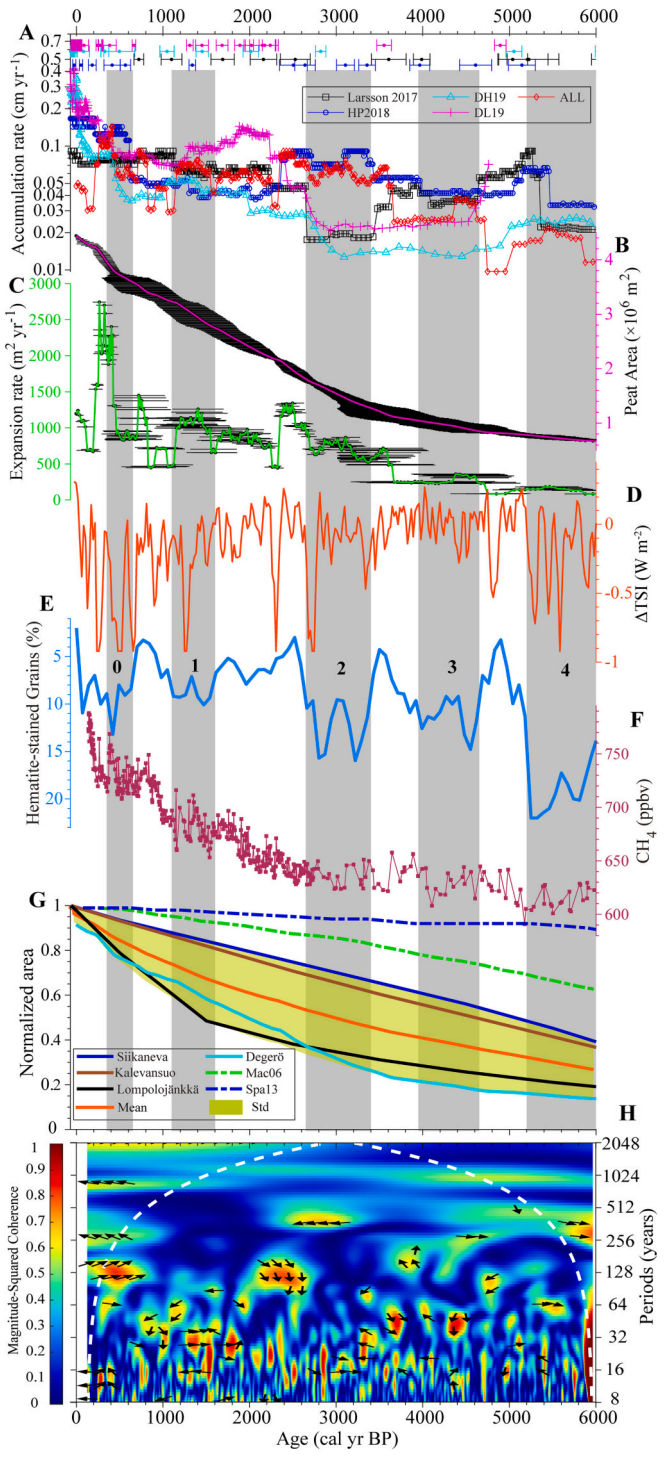

(caption on next column)

Fig. 6. Time series of: (A) peat accumulation rates of the 4 cores (Larsson 2017, HP2018, DH19, and DL19) and the reconstruction (ALL) based on them (the raw radiocarbon age-control points are shown as colored points with error bars represent 1σ age range) (B) total peatland area and (C) lateral expansion rate of Degerö (black error bars represent the uncertainties in the age); (D) total solar irradiance anomaly (ΔTSI) reconstruction based on ^{14}C and ^{10}Be contents in ice core and tree ring (Steinhilber et al., 2012); (E) the ice-drifted debris (IRD) record for ocean core MC52-VM29–191 (Bond et al., 1997) (gray bars and the numbers from 1 to 4 designate the Bond events, number 0 indicates the 'Little Ice Age' event); (F) calibrated atmospheric CH_4 concentrations in Arctic ice cores (Beck et al., 2018); (G) normalized peatland area of Degerö, Kalevansuo (Mathijssen et al., 2017), Siikaneva (Mathijssen et al., 2016), Lompolojänkkä (Mathijssen et al., 2014), the average and standard deviation of the 4 peatlands, and the Spa13 peatland area (dashed cyan line) based on the land surface process model (LPX-Bern 1.0) (Spahni et al., 2013) and Mac06 cumulative curve (dashed red line) of the northern peatlands peat initiation probability (MacDonald et al., 2006); (H) wavelet coherence between lateral expansion rate of Degerö Stormyr and atmospheric CH_4 concentration. The direction of the black arrows indicates the phase shift between ecosystem lateral expansion rates and atmospheric CH_4 levels (right: in phase, meaning the timeseries are perfectly correlated; up: lateral expansion rate leads atmospheric CH_4 level by π/2; left: the timeseries are out of phase; down: lateral expansion rate lags by π/2). The white dashed line represents the cone of influence (Torrence and Compo, 1998), beyond which edge effects are abundant, and results should be interpreted with caution.

Ratcliffe et al., 2021), it is expected that this difference may be caused by younger peatlands being underrepresented in the basal age compilation studies. This suggests that the areal extent of northern peatlands before the mid-Holocene might have been overestimated in such previous estimates (Nichols and Peteet, 2019; Treat et al., 2021; Yu et al., 2013). Consequently, the contribution of the lateral expansion of northern peatlands to the global atmospheric CH_4 cycle since the mid-Holocene would thus also be underestimated. In the following paragraphs, we exploratively estimate the impact of northern peatland lateral expansion on atmospheric CH_4 dynamics. We use the assumption that the lateral expansion of four peatlands is a representative sample of northern peatlands. While this is clearly a bold and perhaps questionable assumption to make, we would argue it is more realistic than modelled lateral expansion, based on a disproven assumption of linear growth, which to date have been the primary basis of our understanding of northern peatland lateral dynamics and thus peatland contribution to pre-historical CH_4 concentrations. We recognize this sample size is small but is the best we have available at the current stage (see Section 4.4 for more details). The number of relevant reconstructions in literature is highly limited and we thus urge for more empirical data and multiple cores within peatlands to quantify lateral expansion to further support the hypothesis developed below.

Based on the estimated site-averaged temporal pattern of lateral expansion rate in our synthesis, the peatland area at 6000 cal yr BP was around 35 % of the pre-industrial level (Fig. 6F). Taking the area of northern peatlands to be 4.0×10^6 km^2 (Gorham, 1991; Yu et al., 2010), it is estimated that around 2.64×10^6 km^2 of peatland area was newly formed in the northern high latitudes since the mid-Holocene. Given the current or time-averaged median annual CH_4 emission rate of the studied northern peatland being 13.4 g CH_4 m^{-2} yr^{-1} (Nilsson et al., 2008; Turetsky et al., 2014), and unit conversion factor 2.78 Tg CH_4 ppb^{-1} under an 8.4-yr lifetime (Levine et al., 2011; Zürcher et al., 2013), the expansion of northern peatlands since the mid-Holocene could potentially cause an increase of ~35 Tg CH_4 emission. This would correspond to a ~98 ppbv CH_4 perturbation to the atmosphere. Considering the uncertainties in lateral expansion rate and differences in CH_4 emission intensity from peatlands in different hydroclimatic and vegetation conditions, this estimate is surprisingly close to the 100 ppbv 'anomalous' CH_4 rising since the mid-Holocene (Ruddiman and Thomson, 2001). More importantly, the centennial-millennial timescale variations in atmospheric CH_4 concentrations, where a higher increase happened during the late Holocene (after 2500 cal yr BP), are proportionate to the increment of northern peatlands size (Fig. 6F and G). In the light of that the lateral expansion was influenced by hydroclimate variabilities, which could also result in significant changes in the rate of CH_4 emissions, it is plausible that the hydroclimate responsible for the decrease in lateral expansion rate could also cause significant reductions in CH_4 emissions, even as peatland areal extent continued to increase. Therefore, it seems that the 'anomalous' CH_4 rise and the decadal-centennial declines within this rise may be attributed to the general

increase in northern peatland areal extent since the mid-Holocene and the dry/cold climate superimposed on some of the TSI minimums that led to stagnation or reduction in the lateral expansion rate. We thus hypothesize that the lateral expansion of northern peatlands since 5300 cal yr BP may be a significant driver of the 'anomalous' CH_4 rise. Once again, we stress this hypothesis needs more firm empirical support to be fully confirmed.

In contrast to this increased lateral expansion after 5300 cal yr BP, previous studies based on basal age compilations suggested that the peat areal extent of northern peatlands at 5300 cal yr BP was at least already 80 % of its current extent (Loisel et al., 2017; MacDonald et al., 2006; Treat et al., 2016; Yu et al., 2010). The remaining 20 % increase in northern peatland extent could only cause a ~ 40 ppbv CH_4 perturbation to the atmosphere. This may explain why Treat et al. (2021) found the northern peatland was nearly completely decoupled from the trend in atmospheric CH_4 concentration throughout the Holocene. However, if the lateral expansion pattern estimated from our compilation (Fig. 6G) would have been used, it is alternatively plausible that the northern peatlands were <40 % of their present areal extent before the mid-Holocene. Therefore, the increment of northern peatland extent and its lateral expansion processes could be more strongly coupled with atmospheric CH_4 concentration variations during the late Holocene than that of early Holocene.

Notwithstanding the mentioned necessary assumptions and extrapolation due to limited data availability, our exploratory finding supports the hypothesis of Blunier et al. (1995), that the increased atmospheric CH_4 concentration in the mid-Holocene was caused by an increasing contribution from northern wetlands (Blunier et al., 1995). Because the CH_4 emitted from peatlands/wetlands is more depleted in $\delta^{13}CH_4$ than that from geological sources, $\delta^{13}CH_4$ signals are widely used in tracing its sources (Conrad, 2005; Fisher et al., 2017; Nisbet et al., 2016). Recent studies have shown that CH_4 emitted from high-latitude peatlands/wetlands was more depleted in $\delta^{13}CH_4$ than that from tropical and temperate regions (Fisher et al., 2017; Guo et al., 2021). It is thus expected that the atmospheric CH_4 is relatively depleted in $\delta^{13}C$ when there were more emissions from the northern peatlands. Interestingly, it has been noted that atmospheric CH_4 rising since the MWP was accompanied by continuous depletion in $\delta^{13}CH_4$ (Ferretti et al., 2005; Sowers, 2010). These observations are in concert with enhanced CH_4 emissions from northern peatlands after the mid-Holocene due to intensified lateral expansion, further supporting our speculation.

By examining the contribution of northern peatlands to CH_4 emissions in relation to the abrupt atmospheric CH_4 concentration declining during the 8.2 kyr cooling event, Zürcher et al. (2013) found that CH_4 emissions originating from northern peatlands could only explain 23 % of the observed decline. This suggests that the contribution of northern peatland CH_4 emission to the atmospheric CH_4 concentration is still small before the mid-Holocene. It has been proposed that intensified tropical wetlands CH_4 emission could be the main driver of the 'anomalous' increase (Singarayer et al., 2011). However, the megadrought at around 4000 cal yr BP recorded in the low latitudes (Blunier et al., 1995; Peng et al., 2021a) contradicts the fact that atmospheric CH_4 was rising by that period (Fig. 6D), suggesting this hypothesis needs verification. Our results indicate that the increment of peat areal extent in the northern peatland may be a key factor controlling the 'anomalous' atmospheric CH_4 rising since the mid-Holocene, as revealed by the consistent synchrony in atmospheric CH_4 concentration and peatland lateral expansion dynamics.

Our results, corroborated by supplementary data from other sites, support the hypothesis of northern peatlands as major source of atmospheric CH_4since the mid-Holocene (Blunier et al., 1995). Although anthropogenic early rice paddy cultivation (Ruddiman et al., 2008), Hudson Bay Lowlands' peatland initiation (Packalen et al., 2014), and increased tropical wetland emissions (Chappellaz et al., 1997; Singarayer et al., 2011) have been invoked as dominant controls on the mid-Holocene atmospheric CH_4 rising. We propose that if other northern peatlands follow the same expansion pattern seen here in our analysis, the non-linear lateral expansion could be a plausible driver of the atmospheric CH_4 increase since the mid-Holocene, rather than early anthropogenic (Ruddiman, 2003; Ruddiman et al., 2008) or Southern Hemisphere tropical wetland (Singarayer et al., 2011) emissions.

4.3. Millennial timescale paludification and spatial heterogeneity of peat thickness

Peatland lateral expansion rates have been incorporated into several studies focusing on long-term carbon exchange dynamics (Korhola, 1994; Mathijssen et al., 2014; Mathijssen et al., 2017; Ruppel et al., 2013). In these studies, multiple basal peat dating samples within one peatland were used to reconstruct the millennial timescale lateral expansion of the peatland (Korhola, 1994; Mathijssen et al., 2014). However, the use of this method in large-scale peatland complexes is often compromised by a high degree of spatial heterogeneity in peat depth due to underlying topography, which is usually not well-constrained due to limited sampling sites and peat thickness measurements (Korhola et al., 1996). Our measurements with high sampling density show that peat thickness varies considerably in space (Fig. 4). We accounted for such heterogeneity by extracting peatland areas at different peat depths using a high-resolution peat thickness model based on GPR measurements. Next, we reconstruct historical peatland areas by combining the area-depth result with an age-depth model based on 89 $AMS^{14}C$ dates of macrofossil samples from four peat cores (Table S1) (Larsson et al., 2017; Nilsson et al., 2001). By doing so, not only the temporal evolution of peatland area and the lateral expansion rate, both horizontal and vertical, could be estimated (Fig. 6A and B), but also the likely spatial progression of peatland development can be illustrated (Fig. 7). In comparison with previous studies using basal ages for reconstructing millennial timescale peatland developments during the Holocene (Korhola, 1994; Mathijssen et al., 2017; Mathijssen et al., 2022), our GPR-based reconstruction can provide a more nuanced understanding of the dynamics in the peatland lateral expansion processes both temporally and spatially.

Our reconstructions show peatland distribution in Degerö was scattered in multiple isolated pockets before the mid-Holocene (Fig. 7), pointing to peat initiation in landscape depressions at which terrestrialization took place. From these isolated pockets, paludification was the dominant peat-forming and lateral expansion mechanism after the mid-Holocene (Malmström, 1923). The individual small peatland basins at Degerö coalesced into a single large peatland complex at around 2000 cal yr BP, similar to the Siikaneva peatland complex (Mathijssen et al., 2016), but different from the smaller peatlands such as Reksuo (Korhola et al., 1996; Korhola, 1994) and Lompolojänkkä (Mathijssen et al., 2014). The paludification of Degerö from 6000 to 1000 cal yr BP has a southeast-northwest directionality (Fig. 7), which is consistent with the dominant direction of post-glacial landforms and drainage networks in the region (Ehnvall et al., 2023; Hoppe, 1959), which could be likely caused the flatter surface topography in this direction as revealed by LiDAR-derived Digital Elevation Model (DEM) (Fig. 1B) (Leach et al., 2016). This directionality constrained by underlying topography is an important consideration that has perhaps been overlooked in previous studies identifying the role of slope in regulating growth rates and estimating peatland lateral expansion rate only based on single or few directions of transect analysis (Almquist-Jacobson and Foster, 1995; Granlund et al., 2022; Loisel et al., 2013; Juselius-Rajamäki et al., 2023). Directionality of post-glacial landforms is something that would ideally be incorporated into models of high latitude peatland expansion in the future.

4.4. Uncertainties and recommendations

Though a detailed spatial peatland progression through time was reconstructed in this study, uncertainties in peat basal ages and the age-

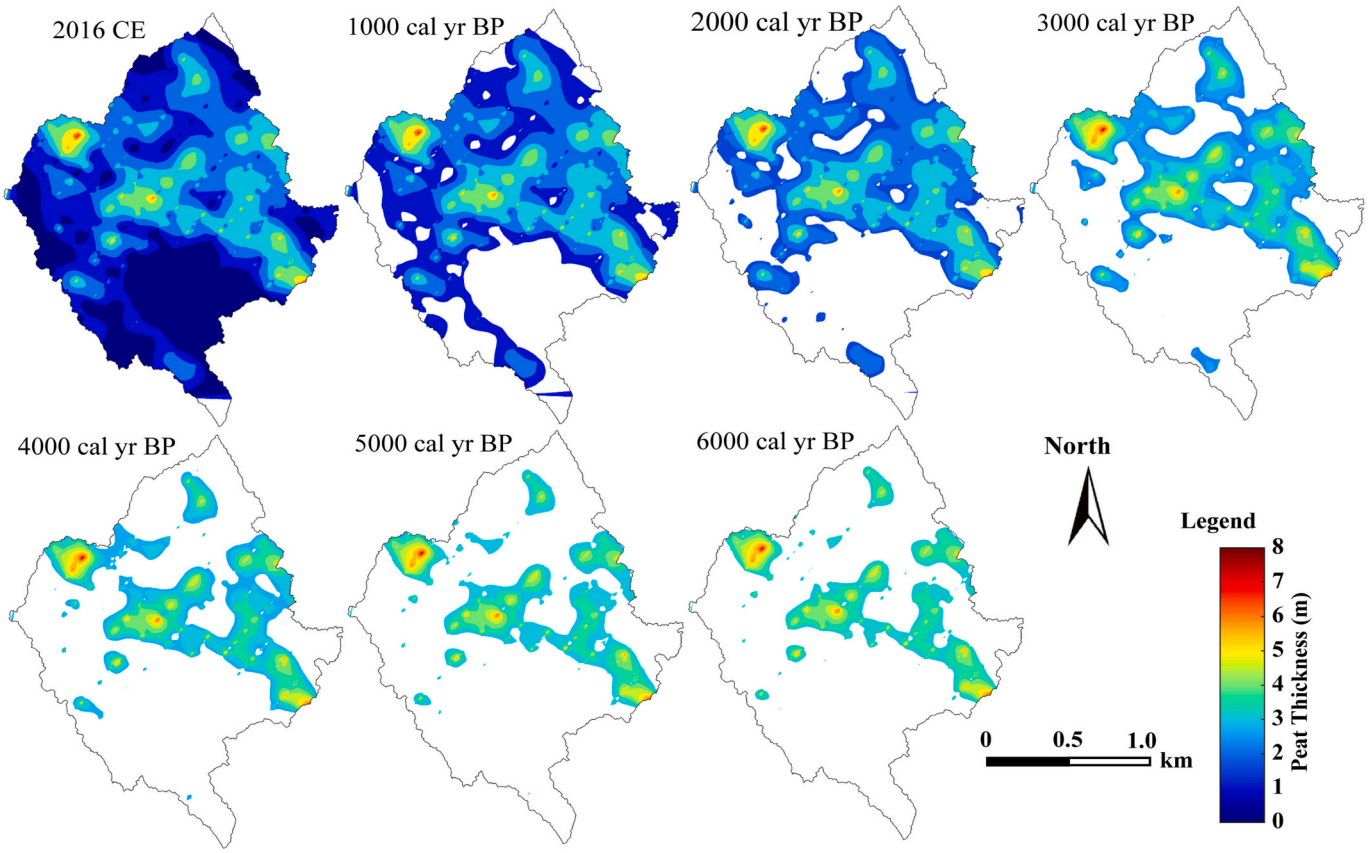

Fig. 7. Maps showing the peatland that developed during each time slice in the current catchment of Degerö Stormyr peatland complex.

depth model could not be well addressed due to the heterogeneities in peat accumulation through time and space. It is well understood that the age-depth relationship may vary by several hundreds to thousand years across different points in a mire (Korhola, 1994; Piilo et al., 2020). Multiple spatially well-distributed age-depth models are ideally needed for a more precise understanding of peatland lateral expansion, which due to high expenses are extremely scarce. Our estimate, therefore, inevitably comes with an uncertainty of several hundred to thousand years as well. However, the strong agreement between our lateral expansion rate and that of other intensively dated peatlands is encouraging and supports the calculated expansion rate of Degerö to be close to the mean climate-controlled expansion rate of northern peatlands (Fig. 6G), despite the uncertainty in age. Among other reasons, this study stresses the data scarcity of, and research needs for, site-specific peatland lateral expansion reconstructions. More information, such as multiple age-depth models for peatlands in different hydroclimatic and geomorphological settings, is needed to validate our hypothesis for the northern peatlands.

5. Conclusion

We reconstructed the 6000-year peatland lateral expansion history of a peatland complex in northern Sweden, based on 89 AMS ^{14}C dates from four peat cores and high-resolution Ground Penetrating Radar (GPR) peat thickness measurements along 25 km of transects. Based on our analysis, rapid lateral expansion of the peatland seems to have occurred after around 3500 cal yr BP. Accelerated lateral expansion occurred during the Medieval Warm Period and after the little ice age. Abrupt declines in both atmospheric CH_4 concentration and peatland lateral expansion rates are found to coincide with ice-rafted debris events and increased total solar irradiance. Further synthesis of lateral expansion data from four Fennoscandian peatlands suggests that over around 60 % of the northern peatland area incrementally expanded through lateral growth from existing peatlands after the mid-Holocene. This expansion could have caused an increase of approximately 100 ppbv CH_4 in the atmosphere since then. In turn, this dynamic increment of the northern peatland area was in concert with the 'anomalous' increase of atmospheric CH_4 concentrations after the mid-Holocene. Based on these analyses, we speculate that northern high latitudes and global hydroclimatic changes have been dominant drivers of both peatland expansion and the global carbon cycle since the mid-Holocene. Nevertheless, we stress that there is currently too little empirical support available to fully test this hypothesis. Thus, we recommend that more studies are made where multiple peat cores taken from within the same peatland are dated. This study highlights the dynamic nature of lateral expansion processes in northern peatlands and emphasizes that their climatic controls are likely important drivers of the mid-Holocene 'anomalous' increase in atmospheric CH_4 concentrations.

CRediT authorship contribution statement

Haijun Peng: Conceptualization, Funding acquisition, Sampling, Writing – original draft. Jelmer J. Nijp: Data Processing, Writing – original draft. Joshua L. Ratcliffe: Conceptualization, Writing – original draft. Chuxian Li: Sampling, Writing - Review & Editing. Bing Hong: Funding acquisition, Writing - Review & Editing. William Lidberg: Writing - Review & Editing. Mengxiu Zeng: Methodology, Data Curation. Dmitri Mauquoy: Resources, Writing – original draft. Kevin Bishop: Resources, Sampling. Mats B. Nilsson: Conceptualization, Funding acquisition, Sampling, Resources. All authors interpreted and discussed the ideas and results and contributed to writing the final manuscript.

Declaration of competing interest

The authors declare that they have no known competing financial interests or personal relationships that could have appeared to influence the work reported in this paper.

Data availability

Data will be made available on request.

Acknowledgments

This research was supported by the National Natural Science Foundation of China (grant numbers: 41907288, 41773140, and 42007400), the Strategic Priority Research Program of Chinese Academy of Sciences (grant number: XDB40000000), the Swedish Research Council VR project (grant numbers: 2018-03966), and the Swedish Infrastructure for Ecosystem Science (SITES). Martin Hjärten is acknowledged for planning, field data collection, and post processing of the GPR raw data. Thomas Hörnlund is acknowledged for careful field assistance.

Appendix A. Supplementary data

Supplementary data to this article can be found online at https://doi.org/10.1016/j.scitotenv.2023.168450.

References

Adrian, N., 2004. Ground-penetrating radar and its use in sedimentology: principles, problems and progress. Earth Sci. Rev. 66, 261–330.
Almquist-Jacobson, H., Foster, D.R., 1995. Toward an integrated model for raised-bog development: theory and field evidence. Ecology 76, 2503–2516.
Baumgartner, M., Schilt, A., Eicher, O., Schmitt, J., Schwander, J., Spahni, R., Fischer, H., Stocker, T.F., 2012. High-resolution interpolar difference of atmospheric methane around the Last Glacial Maximum. Biogeosciences 9, 3961–3977.
Beck, J., Bock, M., Schmitt, J., Seth, B., Blunier, T., Fischer, H., 2018. Bipolar carbon and hydrogen isotope constraints on the Holocene methane budget. Biogeosciences 15, 7155–7175.
Blaauw, M., Christen, J.A., 2011. Flexible paleoclimate age-depth models using an autoregressive gamma process. Bayesian Anal. 6, 457–474.
Blunier, T., Chappellaz, J., Schwander, J., Stauffer, B., Raynaud, D., 1995. Variations in atmospheric methane concentration during the Holocene epoch. Nature 374, 46–49.
Bock, M., Schmitt, J., Beck, J., Seth, B., Chappellaz, J., Fischer, H., 2017. Glacial/interglacial wetland, biomass burning, and geologic methane emissions constrained by dual stable isotopic CH_4 ice core records. Proc. Natl. Acad. Sci. 114, E5778–E5786.
Bond, G., Showers, W., Cheseby, M., Lotti, R., Almasi, P., deMenocal, P., Priore, P., Cullen, H., Hajdas, I., Bonani, G., 1997. A pervasive millennial-scale cycle in North Atlantic Holocene and glacial climates. Science 278, 1257–1266.
Campbell, I.D., Campbell, C., Yu, Z., Vitt, D.H., Apps, M.J., 2000. Millennial-scale rhythms in peatlands in the western interior of Canada and in the global carbon cycle. Quat. Res. 54, 155–158.
Chappellaz, J., Barnola, J., Raynaud, D., Korotkevich, Y.S., Lorius, C., 1990. Ice-core record of atmospheric methane over the past 160,000 years. Nature 345, 127–131.
Chappellaz, J., Bluniert, T., Raynaud, D., Barnola, J.M., Schwander, J., Stauffert, B., 1993. Synchronous changes in atmospheric CH4 and Greenland climate between 40 and 8 kyr BP. Nature 366, 443–445.
Chappellaz, J., Blunier, T., Kints, S., Dällenbach, A., Barnola, J.-M., Schwander, J., Raynaud, D., Stauffer, B., 1997. Changes in the atmospheric CH_4 gradient between Greenland and Antarctica during the Holocene. J. Geophys. Res. Atmos. 102, 15987–15997.
Charman, D.J., Beilman, D.W., Blaauw, M., Booth, R.K., Brewer, S., Chambers, F.M., Christen, J.A., Gallego-Sala, A., Harrison, S.P., Hughes, P.D.M., Jackson, S.T., Korhola, A., Mauquoy, D., Mitchell, F.J.G., Prentice, I.C., Van Der Linden, M., De Vleeschouwer, F., Yu, Z.C., Alm, J., Bauer, I.E., Corish, Y.M.C., Garneau, M., Hohl, V., Huang, Y., Karofeld, E., Le Roux, G., Loisel, J., Moschen, R., Nichols, J.E., Nieminen, T.M., Macdonald, G.M., Phadtare, N.R., Rausch, N., Sillasoo, Ü., Swindles, G.T., Tuittila, E.S., Ukonmaanaho, L., Väliranta, M., Van Bellen, S., Van Geel, B., Vitt, D.H., Zhao, Y., 2013. Climate-related changes in peatland carbon accumulation during the last millennium. Biogeosciences 10, 929–944.
Comas, X., Slater, L., Reeve, A., 2005. Geophysical and hydrological evaluation of two bog complexes in a northern peatland: implications for the distribution of biogenic gases at the basin scale. Glob. Biogeochem. Cycles 19.
Conrad, R., 2005. Quantification of methanogenic pathways using stable carbon isotopic signatures: a review and a proposal. Org. Geochem. 36, 739–752.
Dommain, R., Couwenberg, J., Glaser, P.H., Joosten, H., Suryadiputra, I.N.N., 2014. Carbon storage and release in Indonesian peatlands since the last deglaciation. Quat. Sci. Rev. 97, 1–32.
Edvardsson, J., Poska, A., Van der Putten, N., Rundgren, M., Linderson, H., Hammarlund, D., 2014. Late-Holocene expansion of a south Swedish peatland and its impact on marginal ecosystems: evidence from dendrochronology, peat stratigraphy and palaeobotanical data. The Holocene 24, 466–476.
Ehnvall, B., Ratcliffe, J.L., Bohlin, E., Nilsson, M.B., Öquist, M.G., Sponseller, R.A., Grabs, T., 2023. Landscape constraints on mire lateral expansion. Quat. Sci. Rev. 302, 107961.
Etminan, M., Myhre, G., Highwood, E.J., Shine, K.P., 2016. Radiative forcing of carbon dioxide, methane, and nitrous oxide: a significant revision of the methane radiative forcing. Geophys. Res. Lett. 43, 12,614–612,623.
Ferretti, D.F., Miller, J.B., White, J.W.C., Etheridge, D.M., Lassey, K.R., Lowe, D.C., Meure, C.M.M., Dreier, M.F., Trudinger, C.M., van Ommen, T.D., Langenfelds, R.L., 2005. Unexpected changes to the global methane budget over the past 2000 years. Science 309, 1714–1717.
Fisher, R.E., France, J.L., Lowry, D., Lanoisellé, M., Brownlow, R., Pyle, J.A., Cain, M., Warwick, N., Skiba, U.M., Drewer, J., Dinsmore, K.J., Leeson, S.R., Bauguitte, S.J.B., Wellpott, A., O'Shea, S.J., Allen, G., Gallagher, M.W., Pitt, J., Percival, C.J., Bower, K., George, C., Hayman, G.D., Aalto, T., Lohila, A., Aurela, M., Laurila, T., Crill, P.M., McCalley, C.K., Nisbet, E.G., 2017. Measurement of the ^{13}C isotopic signature of methane emissions from northern European wetlands. Glob. Biogeochem. Cycles 31, 2016GB005504.
Fletcher, E.M.S., Tans, P.P., Bruhwiler, L.M., Miller, J.B., Heimann, M., 2004. CH4 sources estimated from atmospheric observations of CH_4 and its $^{13}C/^{12}C$ isotopic ratios: 1. Inverse modeling of source processes. Glob. Biogeochem. Cycles 18.
Frolking, S., Roulet, N.T., 2007. Holocene radiative forcing impact of northern peatland carbon accumulation and methane emissions. Glob. Chang. Biol. 13, 1079–1088.
Gorham, E., 1991. Northern peatlands: role in the carbon cycle and probable responses to climatic warming. Ecol. Appl. 1, 182–195.
Gorham, E., Lehman, C., Dyke, A., Clymo, D., Janssens, J., 2012. Long-term carbon sequestration in North American peatlands. Quat. Sci. Rev. 58, 77–82.
Granlund, L., Vesakoski, V., Sallinen, A., Kolari, T.H.M., Wolff, F., Tahvanainen, T., 2022. Recent lateral expansion of Sphagnum bogs over central fen areas of boreal Aapa mire complexes. Ecosystems 25 (7), 1455–1475.
Guo, Q., Peng, H., Hong, B., Yao, H., Zhu, Y., Ding, H., An, N., Hong, Y., 2021. Variations of methane stable isotopic values from an Alpine peatland on the eastern Qinghai-Tibetan Plateau. Acta Geochim. 40, 473–483.
Holmquist, J.R., MacDonald, G.M., 2014. Peatland succession and long-term apparent carbon accumulation in central and northern Ontario, Canada. The Holocene 24, 1075–1089.
Hopcroft, P.O., Valdes, P.J., O'Connor, F.M., Kaplan, J.O., Beerling, D.J., 2017. Understanding the glacial methane cycle. Nat. Commun. 8, 14383.
Hoppe, G., 1959. Glacial morphology and inland ice recession in northern Sweden. Geogr. Ann. 41, 193–212.
Hugelius, G., Loisel, J., Chadburn, S., Jackson, R.B., Jones, M., MacDonald, G., Marushchak, M., Olefeldt, D., Packalen, M., Siewert, M.B., Treat, C., Turetsky, M., Voigt, C., Yu, Z., 2020. Large stocks of peatland carbon and nitrogen are vulnerable to permafrost thaw. Proc. Natl. Acad. Sci. 117 (34), 20438–20446.
Ivanov, K.E.e, 1981. Water Movement in Mirelands. Academic Press Inc. (London) Ltd.
Juselius-Rajamäki, T., Väliranta, M., Korhola, A., 2023. The ongoing lateral expansion of peatlands in Finland. Glob. Chang. 1–19. https://doi.org/10.1111/gcb.16988.
Kirschke, S., Bousquet, P., Ciais, P., Saunois, M., Canadell, J.G., Dlugokencky, E.J., Bergamaschi, P., Bergmann, D., Blake, D.R., Bruhwiler, L., Cameron-Smith, P., Castaldi, S., Chevallier, F., Feng, L., Fraser, A., Heimann, M., Hodson, E.L., Houweling, S., Josse, B., Fraser, P.J., Krummel, P.B., Lamarque, J.-F., Langenfelds, R. L., Le Quere, C., Naik, V., O'Doherty, S., Palmer, P.I., Pison, I., Plummer, D., Poulter, B., Prinn, R.G., Rigby, M., Ringeval, B., Santini, M., Schmidt, M., Shindell, D. T., Simpson, I.J., Spahni, R., Steele, L.P., Strode, S.A., Sudo, K., Szopa, S., van der Werf, G.R., Voulgarakis, A., van Weele, M., Weiss, R.F., Williams, J.E., Zeng, G., 2013. Three decades of global methane sources and sinks. Nat. Geosci. 6, 813–823.
Konijnendijk, T.Y.M., Weber, S.L., Tuenter, E., van Weele, M., 2011. Methane variations on orbital timescales: a transient modeling experiment. Clim. Past 7, 635–648.
Korhola, A.A., 1994. Radiocarbon evidence for rates of lateral expansion in raised mires in southern Finland. Quat. Res. 42, 299–307.
Korhola, A., Alm, J., Tolonen, K., Turunen, J., Jungner, H., 1996. Three-dimensional reconstruction of carbon accumulation and CH4 emission during nine millennia in a raised mire. J. Quat. Sci. 11.
Korhola, A., Ruppel, M., Seppä, H., Väliranta, M., Virtanen, T., Weckström, J., 2010. The importance of northern peatland expansion to the late-Holocene rise of atmospheric methane. Quat. Sci. Rev. 29, 611–617.
Kulczyński, 1949. Peat bogs of Polesie. In: Cracovie: Academie Polonaise des Sciences et des Lettres.
Larsson, A., Segerström, U., Laudon, H., Nilsson, M.B., 2017. Holocene carbon and nitrogen accumulation rates in a boreal oligotrophic fen. The Holocene 27, 811–821.
Leach, J.A., Larsson, A., Wallin, M.B., Nilsson, M.B., Laudon, H., 2016. Twelve year interannual and seasonal variability of stream carbon export from a boreal peatland catchment. J. Geophys. Res. Biogeosci. 121, 1851–1866.
Levine, J.G., Wolff, E.W., Jones, A.E., Sime, L.C., Valdes, P.J., Archibald, A.T., Carver, G. D., Warwick, N.J., Pyle, J.A., 2011. Reconciling the changes in atmospheric methane sources and sinks between the Last Glacial Maximum and the pre-industrial era. Geophys. Res. Lett. 38.
Li, C., Jiskra, M., Nilsson, M.B., Osterwalder, S., Zhu, W., Mauquoy, D., Skyllberg, U., Enrico, M., Peng, H., Song, Y., 2023. Mercury deposition and redox transformation

processes in peatland constrained by mercury stable isotopes. Nat. Commun. https://doi.org/10.1038/s41467-023-43164-8 (Accepted).
Loisel, J., Yu, Z., Parsekian, A., Nolan, J., Slater, L., 2013. Quantifying landscape morphology influence on peatland lateral expansion using ground-penetrating radar (GPR) and peat core analysis. J. Geophys. Res. Biogeosci. 118, 373–384.
Loisel, J., Yu, Z., Beilman, D.W., Camill, P., Alm, J., Amesbury, M.J., Anderson, D., Andersson, S., Bochicchio, C., Barber, K., 2014. A database and synthesis of northern peatland soil properties and Holocene carbon and nitrogen accumulation. Holocene 24, 1028–1042.
Loisel, J., van Bellen, S., Pelletier, L., Talbot, J., Hugelius, G., Karran, D., Yu, Z., Nichols, J., Holmquist, J., 2017. Insights and issues with estimating northern peatland carbon stocks and fluxes since the Last Glacial Maximum. Earth Sci. Rev. 165, 59–80.
MacDonald, G.M., Beilman, D.W., Kremenetski, K.V., Sheng, Y., Smith, L.C., Velichko, A. A., 2006. Rapid early development of circumarctic peatlands and atmospheric CH_4 and CO_2 variations. Science 314, 285–288.
Malmström, C., 1923. Degerö stormyr: en botanisk, hydrologisk och utvecklingshistorisk undersökning över ett nordsvenskt myrkomplex. Centraltryckeriet.
Mathijssen, P., Tuovinen, J.P., Lohila, A., Aurela, M., Juutinen, S., Laurila, T., Niemelä, E., Tuittila, E.S., Väliranta, M., 2014. Development, carbon accumulation, and radiative forcing of a subarctic fen over the Holocene. Holocene 24, 1156–1166.
Mathijssen, P.J.H., Väliranta, M., Korrensalo, A., Alekseychik, P., Vesala, T., Rinne, J., Tuittila, E.-S., 2016. Reconstruction of Holocene carbon dynamics in a large boreal peatland complex, southern Finland. Quat. Sci. Rev. 142, 1–15.
Mathijssen, P.J.H., Kähkölä, N., Tuovinen, J.-P., Lohila, A., Minkkinen, K., Laurila, T., Väliranta, M., 2017. Lateral expansion and carbon exchange of a boreal peatland in Finland resulting in 7000 years of positive radiative forcing. J. Geophys. Res. Biogeosci. 122, 562–577.
Mathijssen, P.J.H., Tuovinen, J.-P., Lohila, A., Väliranta, M., Tuittila, E.-S., 2022. Identifying main uncertainties in estimating past and present radiative forcing of peatlands. Glob. Chang. Biol. 28 (13), 4069–4084.
Morris, P.J., Swindles, G.T., Valdes, P.J., Ivanovic, R.F., Gregoire, L.J., Smith, M.W., Tarasov, L., Haywood, A.M., Bacon, K.L., 2018. Global peatland initiation driven by regionally asynchronous warming. Proc. Natl. Acad. Sci. 115, 4851–4856.
Nichols, J.E., Peteet, D.M., 2019. Rapid expansion of northern peatlands and doubled estimate of carbon storage. Nat. Geosci. 12, 917–921.
Nijp, J.J., Metselaar, K., Limpens, J., Bartholomeus, H.M., Nilsson, M.B., Berendse, F., Zee, S.E.A.T.M., 2019. High-resolution peat volume change in a northern peatland: spatial variability, main drivers, and impact on ecohydrology. Ecohydrology 12.
Nilsson, M., Klarqvist, M., Bohlin, E., Possnert, G., 2001. Variation in ^{14}C age of macrofossils and different fractions of minute peat samples dated by AMS. Holocene 11, 579–586.
Nilsson, M., Sagerfors, J., Buffam, I., Laudon, H., Eriksson, T., Grelle, A., Klemedtsson, L., Weslien, P., Lindroth, A., 2008. Contemporary carbon accumulation in a boreal oligotrophic minerogenic mire - a significant sink after accounting for all C-fluxes. Glob. Chang. Biol. 14, 2317–2332.
Nisbet, E.G., Dlugokencky, E.J., Manning, M.R., Lowry, D., Fisher, R.E., France, J.L., Michel, S.E., Miller, J.B., White, J.W.C., Vaughn, B., 2016. Rising atmospheric methane: 2007-2014 growth and isotopic shift. Glob. Biogeochem. Cycles 30.
Olid, C., Nilsson, M.B., Eriksson, T., Klaminder, J., 2014. The effects of temperature and nitrogen and sulfur additions on carbon accumulation in a nutrient-poor boreal mire: decadal effects assessed using 210Pb peat chronologies. J. Geophys. Res. Biogeosci. 119, 392–403.
Packalen, M.S., Finkelstein, S.A., McLaughlin, J.W., 2014. Carbon storage and potential methane production in the Hudson Bay Lowlands since mid-Holocene peat initiation. Nat. Commun. 5, 4078.
Payne, R.J., Ratcliffe, J., Andersen, R., Flitcroft, C.E., 2016. A meta-database of peatland palaeoecology in Great Britain. Palaeogeogr. Palaeoclimatol. Palaeoecol. 457, 389–395.
Peichl, M., Öquist, M., Ottosson Löfvenius, M., Ilstedt, U., Sagerfors, J., Grelle, A., Lindroth, A., Nilsson, M.B., 2014. A 12-year record reveals pre-growing season temperature and water table level threshold effects on the net carbon dioxide exchange in a boreal fen. Environ. Res. Lett. 9, 055006.
Peng, H., Bao, K., Yuan, L., Uchida, M., Cai, C., Zhu, Y., Hong, B., Guo, Q., Ding, H., Yao, H., Hong, Y., 2021a. Abrupt climate variability since the last deglaciation based on a high-resolution peat dust deposition record from southwest China. Quat. Sci. Rev. 252, 106749.
Peng, H., Chi, J., Yao, H., Guo, Q., Hong, B., Ding, H., Zhu, Y., Wang, J., Hong, Y., 2021b. Methane emissions offset net carbon dioxide uptake from an alpine peatland on the Eastern Qinghai-Tibetan Plateau. J. Geophys. Res. Atmos. 126 (19), e2021JD034671.
Piilo, S.R., Korhola, A., Heiskanen, L., Tuovinen, J.-P., Aurela, M., Juutinen, S., Marttila, H., Saari, M., Tuittila, E.-S., Turunen, J., Väliranta, M.M., 2020. Spatially varying peatland initiation, Holocene development, carbon accumulation patterns and radiative forcing within a subarctic fen. Quat. Sci. Rev. 248, 106596.
Ratcliffe, J., Payne, R.J., 2016. Palaeoecological studies as a source of peat depth data: a discussion and data compilation for Scotland. Mires Peat 18.
Ratcliffe, J.L., Peng, H., Nijp, J.J., Nilsson, M.B., 2021. Lateral expansion of northern peatlands calls into question a 1,055 GtC estimate of carbon storage. Nature 14 (7), 468–469.
Reyes, A.V., Cooke, C.A., 2011. Northern peatland initiation lagged abrupt increases in deglacial atmospheric CH_4. Proc. Natl. Acad. Sci. 108 (12), 4748–4753.
Ruddiman, W.F., 2003. The anthropogenic greenhouse era began thousands of years ago. Clim. Chang. 61, 261–293.
Ruddiman, W.F., Thomson, J.S., 2001. The case for human causes of increased atmospheric CH_4 over the last 5000 years. Quat. Sci. Rev. 20, 1769–1777.
Ruddiman, W.F., Guo, Z., Zhou, X., Wu, H., Yu, Y., 2008. Early rice farming and anomalous methane trends. Quat. Sci. Rev. 27, 1291–1295.
Ruddiman, W.F., He, F., Vavrus, S.J., Kutzbach, J.E., 2020. The early anthropogenic hypothesis: a review. Quat. Sci. Rev. 240, 106386.
Ruppel, M., Väliranta, M., Virtanen, T., Korhola, A., 2013. Postglacial spatiotemporal peatland initiation and lateral expansion dynamics in North America and northern Europe. The Holocene 23, 1596–1606.
Rydin, H., Jeglum, J.K., Bennett, K.D., 2013. The Biology of Peatlands, 2e. OUP Oxford.
Sallinen, A., Akanegbu, J., Marttila, H., Tahvanainen, T., 2023. Recent and future hydrological trends of aapa mires across the boreal climate gradient. J. Hydrol. 617, 129022.
Sapart, C.J., Monteil, G., Prokopiou, M., van de Wal, R.S.W., Kaplan, J.O., Sperlich, P., Krumhardt, K.M., van der Veen, C., Houweling, S., Krol, M.C., Blunier, T., Sowers, T., Martinerie, P., Witrant, E., Dahl-Jensen, D., Röckmann, T., 2012. Natural and anthropogenic variations in methane sources during the past two millennia. Nature 490, 85–88.
Saunois, M., Stavert, A.R., Poulter, B., Bousquet, P., Canadell, J.G., Jackson, R.B., Raymond, P.A., Dlugokencky, E.J., Houweling, S., Patra, P.K., Ciais, P., Arora, V.K., Bastviken, D., Bergamaschi, P., Blake, D.R., Brailsford, G., Bruhwiler, L., Carlson, K. M., Carrol, M., Castaldi, S., Chandra, N., Crevoisier, C., Crill, P.M., Covey, K., Curry, C.L., Etiope, G., Frankenberg, C., Gedney, N., Hegglin, M.I., Höglund-Isaksson, L., Hugelius, G., Ishizawa, M., Ito, A., Janssens-Maenhout, G., Jensen, K.M., Joos, F., Kleinen, T., Krummel, P.B., Langenfelds, R.L., Laruelle, G.G., Liu, L., Machida, T., Maksyutov, S., McDonald, K.C., McNorton, J., Miller, P.A., Melton, J.R., Morino, I., Müller, J., Murguia-Flores, F., Naik, V., Niwa, Y., Noce, S., O'Doherty, S., Parker, R.J., Peng, C., Peng, S., Peters, G.P., Prigent, C., Prinn, R., Ramonet, M., Regnier, P., Riley, W.J., Rosentreter, J.A., Segers, A., Simpson, I.J., Shi, H., Smith, S. J., Steele, L.P., Thornton, B.F., Tian, H., Tohjima, Y., Tubiello, F.N., Tsuruta, A., Viovy, N., Voulgarakis, A., Weber, T.S., van Weele, M., van der Werf, G.R., Weiss, R. F., Worthy, D., Wunch, D., Yin, Y., Yoshida, Y., Zhang, W., Zhang, Z., Zhao, Y., Zheng, B., Zhu, Q., Zhu, Q., Zhuang, Q., 2020. The global methane budget 2000–2017. Earth Syst. Sci. Data 12, 1561–1623.
Schmidt, G.A., Shindell, D.T., Harder, S., 2004. A note on the relationship between ice core methane concentrations and insolation. Geophys. Res. Lett. 31.
Singarayer, J.S., Valdes, P.J., Friedlingstein, P., Nelson, S., Beerling, D.J., 2011. Late Holocene methane rise caused by orbitally controlled increase in tropical sources. Nature 470, 82–85.
Smith, L.C., MacDonald, G.M., Velichko, A.A., Beilman, D.W., Borisova, O.K., Frey, K.E., Kremenetski, K.V., Sheng, Y., 2004. Siberian peatlands a net carbon sink and global methane source since the early Holocene. Science 303, 353–356.
Sowers, T., 2010. Atmospheric methane isotope records covering the Holocene period. Quat. Sci. Rev. 29, 213–221.
Spahni, R., Joos, F., Stocker, B.D., Steinacher, M., Yu, Z.C., 2013. Transient simulations of the carbon and nitrogen dynamics in northern peatlands: from the Last Glacial Maximum to the 21st century. Clim. Past 9, 1287–1308.
Steinhilber, F., Abreu, J.A., Beer, J., Brunner, I., Christl, M., Fischer, H., Heikkilä, U., Kubik, P.W., Mann, M., McCracken, K.G., Miller, H., Miyahara, H., Oerter, H., Wilhelms, F., 2012. 9,400 years of cosmic radiation and solar activity from ice cores and tree rings. Proc. Natl. Acad. Sci. 109, 5967–5971.
Tanemura, M., Ogawa, T., Ogita, N., 1983. A new algorithm for three-dimensional voronoi tessellation. J. Comput. Phys. 51, 191–207.
Torrence, C., Compo, G.P., 1998. A practical guide to wavelet analysis. Bull. Am. Meteorol. Soc. 79, 61–78.
Treat, C.C., Jones, M.C., Camill, P., Gallego-Sala, A., Garneau, M., Harden, J.W., Hugelius, G., Klein, E.S., Kokfelt, U., Kuhry, P., Loisel, J., Mathijssen, P.J.H., O'Donnell, J.A., Oksanen, P.O., Ronkainen, T.M., Sannel, A.B.K., Talbot, J., Tarnocai, C., Väliranta, M., 2016. Effects of permafrost aggradation on peat properties as determined from a pan-Arctic synthesis of plant macrofossils. J. Geophys. Res. Biogeosci. 121, 78–94.
Treat, C.C., Kleinen, T., Broothaerts, N., Dalton, A.S., Dommain, R., Douglas, T.A., Drexler, J.Z., Finkelstein, S.A., Grosse, G., Hope, G., Hutchings, J., Jones, M.C., Kuhry, P., Lacourse, T., Lähteenoja, O., Loisel, J., Notebaert, B., Payne, R.J., Peteet, D.M., Sannel, A.B.K., Stelling, J.M., Strauss, J., Swindles, G.T., Talbot, J., Tarnocai, C., Verstraeten, G., Williams, C.J., Xia, Z., Yu, Z., Väliranta, M., Hättestrand, M., Alexanderson, H., Brovkin, V., 2019. Widespread global peatland establishment and persistence over the last 130,000 y. Proc. Natl. Acad. Sci. 116, 4822–4827.
Treat, C.C., Jones, M.C., Brosius, L., Grosse, G., Walter Anthony, K., Frolking, S., 2021. The role of wetland expansion and successional processes in methane emissions from northern wetlands during the Holocene. Quat. Sci. Rev. 257, 106864.
Turetsky, M.R., Kotowska, A., Bubier, J., Dise, N.B., Crill, P., Hornibrook, E.R.C., Minkkinen, K., Moore, T.R., Myers-Smith, I.H., Nykänen, H., Olefeldt, D., Rinne, J., Saarnio, S., Shurpali, N., Tuittila, E.-S., Waddington, J.M., White, J.R., Wickland, K. P., Wilmking, M., 2014. A synthesis of methane emissions from 71 northern, temperate, and subtropical wetlands. Glob. Chang. Biol. 20, 2183–2197.
van Bellen, S., Dallaire, P.-L., Garneau, M., Bergeron, Y., 2011. Quantifying spatial and temporal Holocene carbon accumulation in ombrotrophic peatlands of the Eastmain region, Quebec, Canada. Glob. Biogeochem. Cycles 25.
van der Linden, M., Barke, J., Vickery, E., Charman, D.J., van Geel, B., 2008. Late Holocene human impact and climate change recorded in a North Swedish peat deposit. Palaeogeogr. Palaeoclimatol. Palaeoecol. 258, 1–27.
Warner, B.G., Nobes, D.C., Theimer, B.D., 1990. An application of ground penetrating radar to peat stratigraphy of Ellice Swamp, southwestern Ontario. Can. J. Earth Sci. 27, 932–938.
Weckström, J., Seppä, H., Korhola, A., 2010. Climatic influence on peatland formation and lateral expansion in sub-arctic Fennoscandia. Boreas 39, 761–769.

Xing, W., Guo, W., Liang, H., Li, X., Wang, C., He, J., Lu, X., Wang, G., 2016. Holocene peatland initiation and carbon storage in temperate peatlands of the Sanjiang Plain, Northeast China. The Holocene 26, 70–79.
Yu, Z., Loisel, J., Brosseau, P.B., Beilman, D.W., Hunt, S.J., 2010. Global peatland dynamics since the Last Glacial Maximum. Geophys. Res. Lett. 37, 69–73.
Yu, Z., Loisel, J., Turetsky, M.R., Cai, S., Zhao, Y., Frolking, S., MacDonald, G.M., Bubier, J.L., 2013. Evidence for elevated emissions from high-latitude wetlands contributing to high atmospheric CH_4 concentration in the early Holocene. Glob. Biogeochem. Cycles 27, 131–140.
Zhang, Z., Liu, K.-B., Bianchette, T.A., Wang, G., 2018. The mid-Holocene decline of the East Asian summer monsoon indicated by a lake-to-wetland transition in the Sanjiang Plain, Northeast China. The Holocene 28, 246–253.
Zhang, M., Smol, J.P., Bu, Z., 2022. Holocene initiation and expansion of the southern margins of northern peatlands triggered by the East Asian summer monsoon recession. Geosci. Front. 14 (2), 101526.
Zhao, Y., Yu, Z., Tang, Y., Li, H., Yang, B., Li, F., Zhao, W., Sun, J., Chen, J., Li, Q., Zhou, A., 2014. Peatland initiation and carbon accumulation in China over the last 50,000 years. Earth Sci. Rev. 128, 139–146.
Zheng, Y., Fang, Z., Fan, T., Liu, Z., Wang, Z., Li, Q., Pancost, R.D., Naafs, B.D.A., 2019. Operation of the boreal peatland methane cycle across the past 16 k.y. Geology 48, 82–86.
Zürcher, S., Spahni, R., Joos, F., Steinacher, M., Fischer, H., 2013. Impact of an abrupt cooling event on interglacial methane emissions in northern peatlands. Biogeosciences 10, 1963–1981.